Journal of Organometallic Chemistry 908 (2020) 121094

Contents lists available at ScienceDirect

Journal of Organometallic Chemistry

journal homepage: www.elsevier.com/locate/jorganchem

Use of anethole-type ligands to design cytotoxic organometallic ruthenium compounds: An experimental and computational study

Ricardo A. Delgado [a], Antonio Galdámez [b], Catherine Tessini [c], Sebastián Ramírez-Rivera [d], Gisela Aquea [e], Giuliano Bernal [d], Balazs Pinter [f], Franz A. Thomet [a, *]

[a] Laboratory of Organometallics, Department of Chemistry, Universidad Técnica Federico Santa María, Avenida España N°, 1680, Valparaíso, Chile
[b] Department of Chemistry, Faculty of Science, Universidad de Chile, Las Palmeras N° 3425, Ñuñoa, Santiago, Chile
[c] LabQI, Department of Chemistry, Universidad Técnica Federico Santa María, Avenida España N° 1680, Valparaíso, Chile
[d] Laboratory of Molecular and Cellular Biology of Cancer, Department of Biomedical Sciences, Faculty of Medicine, Universidad Católica del Norte, Larrondo N° 1281, Coquimbo, Chile
[e] Laboratory of Biological Chemistry, Institute of Chemistry, Faculty of Sciences, Pontificia Universidad Católica de Valparaíso, Brasil N° 2950, Valparaíso, Chile
[f] Laboratory of Physical Chemistry, Department of Chemistry, Universidad Técnica Federico Santa María, Avenida España N° 1680, Valparaíso, Chile

ARTICLE INFO

Article history:
Received 7 October 2019
Received in revised form
19 December 2019
Accepted 20 December 2019
Available online 23 December 2019

Keywords:
Ru(II) compounds
In vitro cytotoxicity
Hydrolysis
Lipophilicity
Density functional theory

ABSTRACT

Two hitherto unknown organometallic compounds with antitumor activity, [Ru(η^6-2-(1-propenyl)anisole)(en)(Cl)]PF_6 (3) and [Ru(η^6-2-(1-propenyl)anisole)(en)(I)]PF_6 (4), where *en* is ethylenediamine, were synthesized and completely characterized using standard techniques (^{1}H and ^{13}C NMR, high-resolution MS and elemental analysis). The lipophilicity and hydrolysis rate kinetics were assessed and compared to the previously reported [Ru(η^6-4-(1-propenyl)anisole)(en)(halogen)]PF_6 derivatives (4-(1-propenyl)anisole or anethole), where the halogen is Cl (1) or I (2). Based on the obtained rate constants, the coordination of (1-propenyl)anisole to the Ru(en) moiety yielded organometallic compounds that are as active as compounds that bind *p*-cymene as the arene ligand. Consistent with previously reported kinetic data, our density functional theory-based computational study revealed that an associative interchange mechanism predominates in the hydrolysis of this type of compound, and only small variations (~1 kcal mol^{-1}) were observed between the stabilities of the transition states corresponding to different derivatives. *In vitro* analyses of the anti-proliferative activity revealed that compounds 1 to 3 generally exhibit better cytotoxicity and selectivity (tumor versus non tumor cells) toward the gastric tumor cell lines AGS and SNU-1, compared to the parent [Ru(η^6-*p*-cymene)(en)X]PF_6 (X: Cl and I) systems. Compound 3 showed similar cytotoxicity to compound 1 toward the AGS cell line, indicating that the change in the substitution pattern of the coordinated arene from 4-(1-propenyl)anisole to 2-(1-propenyl)anisole did not prominently affect the biological behavior. Compound 2 remained the most promising candidate to treat gastric cancer.

1. Introduction

The therapeutic potential of ruthenium-containing compounds has been investigated since the seventies, and some of the developed Ru(III) complexes, such as KP1019 and NAMI-A (Fig. 1), have reached clinical studies in the past few years [1,2]. The medicinal applications of organometallic Ru(II) species were reported in 1992, initiating a rapid expansion of this field with RAPTA-C and RM175 as lead compounds. This development is chiefly related to the exceptional strength of the Ru(η^6-arene) bond that makes this type of scaffold suitable for aqueous media and the electronic fine tuning of its properties [3–5]. The nature of the arene ligand plays a crucial role in modulating the lipophilicity of the organometallic complex to a great extent and in affecting the kinetics of the aquation process of these molecules [6]. Therefore, the tuning of these properties through ligand decoration and alteration offers a wide scope for further drug design.

For the development of newer derivatives of ruthenium complexes with potential cytotoxic activity, researchers frequently use the commercially available [Ru(η^6-arene)Cl_2]$_2$ dimer, where arene

* Corresponding author.
E-mail address: franz.thomet@usm.cl (F.A. Thomet).

https://doi.org/10.1016/j.jorganchem.2019.121094
0022-328X/

corresponds to *p*-cymene, mesitylene or hexamethylbenzene, as the synthetic precursor to coordinate with different kinds of mono- and bidentate ligands, most of which possess relevant intrinsic biological and/or pharmacological properties [7–10]. In an effort to explore other arene ligands that will produce previously unexplored derivatives with potentially promising biological applications, our research has employed phenylpropanoids such as methyleugenol and estragole as naturally occurring precursors. The coordination of these ligands to ruthenium has enabled us to isolate and test [Ru(η^6-methylisoeugenol)(en)Cl]PF_6 and [Ru(η^6-anethole)(en)Cl]PF_6 (**1**, Fig. 1), in which complex formation also induced the isomerization of the allylic substituent to the 1-propenyl isomer. *In vitro* biological evaluations of the effects of these species on human colon and breast tumor cell lines (HT-29 and MCF-7, respectively) revealed a promising cytotoxicity of compound **1** [11]. The increased biological activity of the latter compound was attributed to the presence of a lower number of polar methoxy substituents on the arene ligand (anethole vs methylisoeugenol), consistent with a previous SAR study of this type of complexes reported by Sadler et al. [12] Further studies of the Ru(η^6-anethole)(en) scaffold showed that the nature of the halide ligand (Cl^-, Br^- or I^-) slightly modifies the *in vitro* cytotoxicity of the system toward HT-29 cells [13]. A significant increase in the biological behavior of the iodide analogue [Ru(η^6-anethole)(en)I]PF_6 (**2**) toward the human gastric tumor cell line AGS was observed [14]. Based on these preliminary findings, the Ru(η^6-anethole)(en) platform is a potent core structure that is worth investigating and developing further.

The present study aims to assess the effects of changing the substitution pattern of the coordinated arene from 4-(1-propenyl) anisole (commonly named anethole) to 2-(1-propenyl)anisole on the chemical properties and cytotoxic activity of the corresponding ruthenium complexes. For this purpose, the commercially available compound 2-allylanisole was employed as the synthetic precursor and the resulting [Ru(η^6-2-(1-propenyl)anisole)(en)X]PF_6 structural isomers, where X = Cl (**3**) or I (**4**), were compared to the previously isolated and characterized compounds **1** and **2** (Scheme 1). Compounds **3** and **4** were completely characterized using ^{1}H and ^{13}C NMR, high-resolution MS and elemental analysis, which are reported here together with an XRD study of compounds **1** and **3**. The lipophilicity and kinetics of hydrolysis were also experimentally determined to establish a predictive relationship between the physicochemical and biological properties of the studied series. The mechanism of hydrolysis was further scrutinized through theoretical calculations. For the assessment of biological activity of these new species, the traditional compounds [Ru(η^6-*p*-cymene)(en)X]PF_6 (X: Cl or I) were also included as controls.

2. Materials and methods

2.1. General considerations

The NMR experiments were performed using an Avance 400 Digital Bruker NMR spectrometer operating at 400.13 MHz for ^{1}H and 100.61 MHz for ^{13}C. Chemical shifts (δ) and coupling constants (J) are reported in ppm and Hz, respectively. The chemical shifts are reported relative to the proton signal of incompletely deuterated DMSO-d_6 (δ 2.49) and the chemical shifts of ^{13}C NMR are reported relative to the carbon of DMSO-d_6 (δ 39.5). The high-resolution mass spectra were recorded using an Exactive™ Plus Orbitrap spectrometer (Thermo Fisher Scientific), and the spectra were obtained in positive mode. The elemental analyses were performed using a Flash EA™ 1112. The $RuCl_3$•xH_2O precursor was purchased from Precious Metals Online, while ethylenediamine (en), KI, 4-allylanisole, 2-allylanisole and [Ru(η^6-*p*-cymene)Cl_2]$_2$ were purchased from Aldrich. [Ru(η^4-1,5-COD)Cl_2]$_n$ and [Ru(η^6-*p*-cymene)(en)X]PF_6, where X is Cl or I, were synthesized using established methods [12,15]. The anhydrous acetonitrile (CaH_2) and hexane (Na) solvents were dried and freshly distilled. All other reagents were obtained from commercial suppliers and were used without further purification.

2.2. X-ray crystallography

The X-ray data were collected at room temperature using a Bruker CCD diffractometer with MoKα radiation. We used Bruker SMART for data collection, data reduction and cell refinement [16], while the SHELXL [17] and Olex2 [18] programs were used to refine the crystal structures. H atoms were placed in geometrically idealized positions and refined using the riding model with *U*iso(H) = 1.2 *U*eq(C) or 1.5 *U*eq(C). Crystal data and details of the structure determination are provided in Table 1. DIAMOND and PLATON programs were utilized to prepare these data for publication [19,20]. CCDC 1894484 and 1894485 contain the supplementary crystallographic data for compounds **1** and **3**. These data can be obtained free of charge at http://www.ccdc.cam.ac.uk/conts/retrieving.html or from the Cambridge Crystallographic Data Centre, 12 Union Road, Cambridge CB2 1EZ, UK; fax: (+44) 1223 336 033; or e-mail: deposit@ccdc.cam.ac.uk.

2.3. Synthesis

2.3.1. Synthesis of the dimeric complex [Ru(η^6-2-(1-propenyl) anisole)Cl_2]$_2$ (*6*)

First, 1.04 g of [Ru(η^4-1,5-COD)Cl_2]$_n$ (3.7 mmol of Ru), 4.25 g of 2-

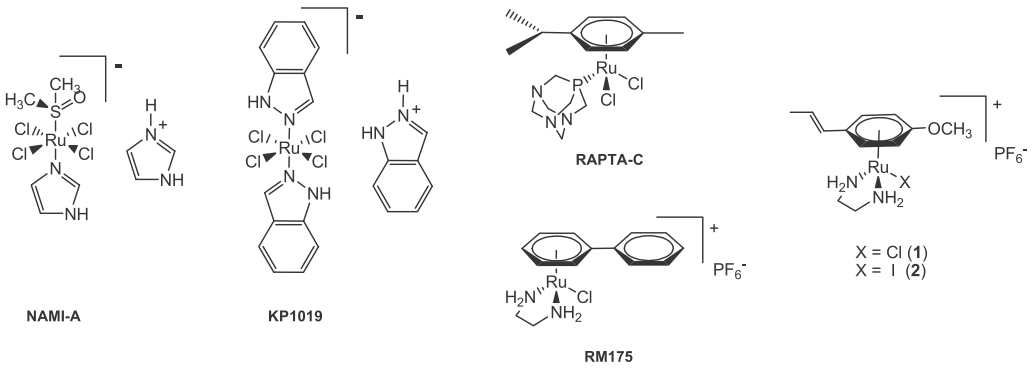

Fig. 1. The structures of NAMI-A, KP1019, RAPTA-C, RM175, [Ru(η^6-anethole)(en)Cl]PF_6 (**1**) and [Ru(η^6-anethole)(en)I]PF_6 (**2**).

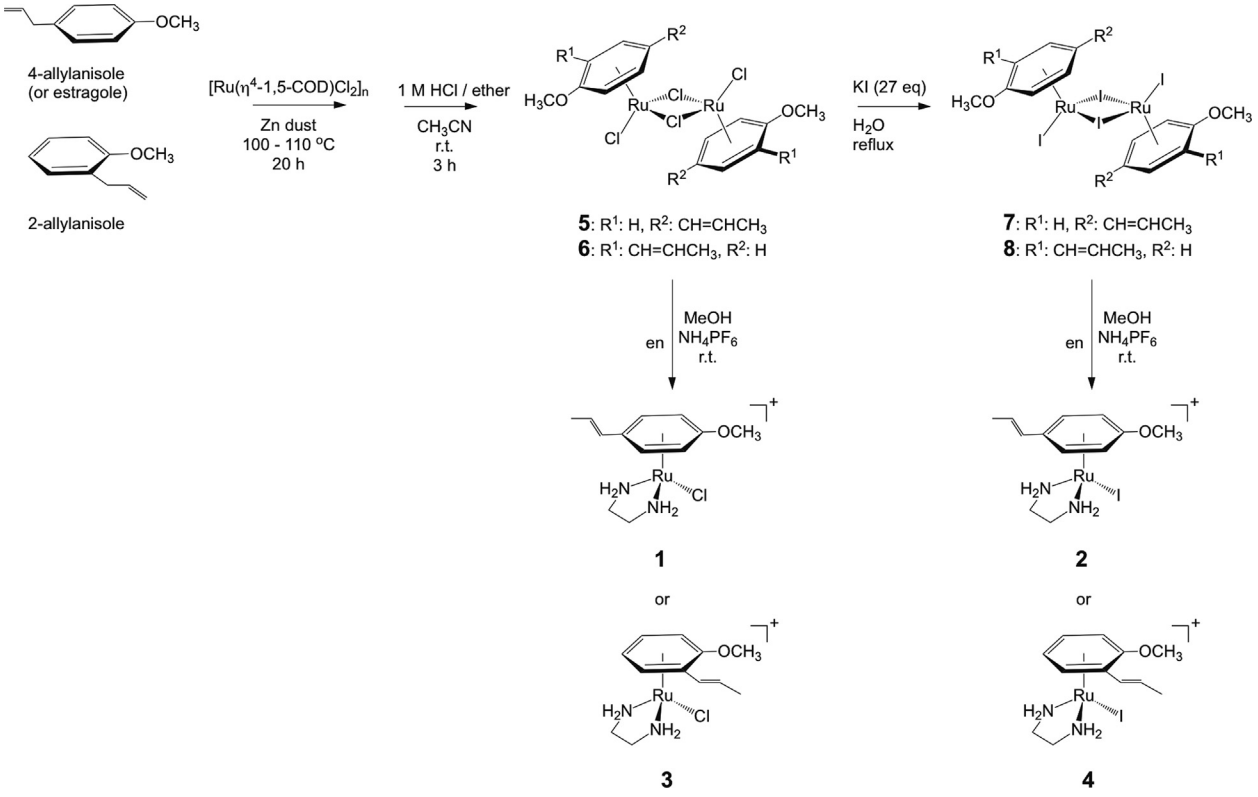

Scheme 1. Synthesis of the organometallic Ru(II) compounds **1** to **4** from free ligands and $[Ru(\eta^4\text{-}1,5\text{-}COD)Cl_2]_n$.

allylanisole (28.7 mmol) and 9.43 g of zinc dust (144 mmol) were added to a dry 100 mL round-bottom flask connected to a dry N_2 inlet. The reaction mixture was heated to 100–110 °C overnight (approximately 20 h). The oily residue was washed with dry hexane (3 × 40 mL). The organic extracts were passed through a glass filter and combined. The organic solvent was removed under a vacuum, and the oily product was redissolved in 5 mL of dry acetonitrile. 40 mL of a 1 M solution of HCl in ether were added, and the mixture was stirred at room temperature for 3 h. The solvents were removed under a vacuum, and the deep red solid was washed with diethyl ether for 30 min (3 × 40 mL). The solid was filtered and dried under a vacuum. 135 mg of $[Ru(\eta^6\text{-}2\text{-}(1\text{-propenyl})anisole)_2Cl_2]_2$ (yield: 11%) were obtained. ^{1}H NMR (DMSO-d_6) δ 1.79 (d, J = 6.4 Hz, 3H, CH═CH–CH_3), 3.93 (s, 3H, OCH_3), 5.34 (dd, J = 5.4 and 5.4 Hz, 1H, Ar-H), 5.67 (d, J = 6.2 Hz, 1H, Ar-H), 6.11 (dd, J = 5.6 and 5.5 Hz, 1H, Ar-H), 6.22 (d, J = 15 Hz, 1H, C*H*═CH–CH_3), 6.32 (d, J = 5.4 Hz, 1H, Ar-H), 6.39 (m, 1H, CH═C*H*–CH_3).

2.3.2. Synthesis of the dimeric complex $[Ru(\eta^6\text{-}2\text{-}(1\text{-propenyl})anisole)I_2]_2$ (**8**)

In a 100 mL round-bottom flask, 140 mg of $[Ru(\eta^6\text{-}(2\text{-}(1\text{-propenyl})anisole)Cl_2]_2$ (0.22 mmol) were dissolved in 30 mL of

Table 1
Crystal data and details of the determination of the structures of compounds **1** and **3**.

Compound	Ru C_{12} H_{20} Cl N_2 O, PF_6(1)	Ru C_{12} H_{20} Cl N_2 O, PF_6(3)
Crystal shape/color	Polyhedron/Orange	Plate/Orange
Crystal size (mm)	0.23 × 0.08 × 0.07	0.27 × 0.21 × 0.06
Crystal system	Monoclinic	Orthorhombic
Space group, Z	$P2_1/n$, 4	Pbca, 8
a (Å)	8.9448(11)	9.6881(8)
b (Å)	17.473(2)	18.4750(15)
c (Å)	11.6552(14)	20.2118(17)
α, β, γ (°)	90, 101.099(2), 90	90, 90, 90
V (Å^3)	1787.6(4)	3617.7(5)
Dcalc (g/cm^{-3})	1.820	1.799
Wavelength, MoKα (Å)	0.71073	
T (K)	298(2)	
F(000)	976	1952
θ-range (°)	2.1< θ < 25.5	2.20 < θ < 23.2
hkl-range	−10: 10; −20: 21; −14: 14	−11: 11; −22: 22; −24: 24
μ (mm^{-1})	1.177	1.163
Reflections collected, R_{int}	13324, 0.044	26662, 0.0334
Observed data [I > 2.0 sigma\(I\)], R_σ	3323, 0.051	3548, 0.0201
Parameters	235	219
R, w$R2$ [$F^2 > 2\sigma(F^2)$]	0.0589, 0.1787	0.0339, 0.1147
Goodness-of-Fit of F^2	0.97	1.073
$\Delta\rho_{max}/\Delta\rho_{min}$ (e Å^{-3})	1.13/−0.95	0.823/−0.445

Milli-Q water. The mixture was refluxed for 3 h, concentrated to the half of volume and filtered. A saturated solution containing 5.9 mmol of KI was added and reacted for 10 min. A violet precipitate appear immediately upon the addition of iodide. The precipitate was washed with water and dried under a vacuum. 118 mg of [Ru(η^6-2-(1-propenyl)anisole)I_2]$_2$ (0.117 mmol, 54% yield) were obtained. ^{1}H NMR (DMSO-d_6) δ 1.82 (d, J = 6.2 Hz, 3H, CH═CH−CH_3), 3.86 (s, 3H, OCH_3), 5.45 (dd, J = 5.4 and 5.3 Hz, 1H, Ar-H), 5.66 (d, J = 6.1 Hz, 1H, Ar-H), 6.27 (m, 2H, Ar-H; CH═CH−CH_3), 6.40 (m, 1H, CH═CH−CH_3), 6.46 (d, J = 5,5 Hz, 1H, Ar-H).

2.3.3. Synthesis of [Ru(η^6-2-(1-propenyl)anisole)(en)Cl]PF_6 (**3**)

In a 100 mL round-bottom flask, 130 mg of [Ru(η^6-2-(1-propenyl)anisole)$_2$$Cl_2$]$_2$ (0.20 mmol) were added to 30 mL of MeOH. 48 μL of ethylenediamine (0.72 mmol) were added to the suspension, and the mixture was stirred at room temperature for 3 h. The reaction mixture was filtrated, and the filtrate was concentrated under a vacuum until 3 mL of solution remained. Afterwards, 165 mg of NH_4PF_6 (1.0 mmol) were added, and the mixture was shaken for 20 min. An orange solid appeared, and the mixture was left at −18 °C for 2 days. The precipitate was filtered, washed with small volumes of diethyl ether (3 × 3 mL) and dried under a vacuum. The product was recrystallized in a mixture of MeOH-ether, finally isolating 58 mg of product (0.118 mmol, 29% yield). ^{1}H NMR (DMSO-d_6) δ 1.79 (d, J = 5.2 Hz, 3H, CH═CH−CH_3), 2.17 (m, 2H, N−CH_2−CH_2−N), 2.24 (m, 1H, N−CH_2−CH_2−N), 2.34 (m, 1H, N−CH_2−CH_2−N), 3.87 (s, 3H, OCH_3), 4.05 (m, 1H, H_2N−C−C−NH_2), 4.29 (m, 1H, H_2N−C−C−NH_2), 5.09 (dd, J = 5.3 and 5.2 Hz, 1H, Ar-H), 5.47 (d, J = 6.1 Hz, 1H, Ar-H), 5.89 (dd, J = 5.5 and 5.5 Hz, 1H, Ar-H), 6.08 (m, 1H, H_2N−C−C−NH_2), 6.15 (m, 2H, Ar-H; H_2N−C−C−NH_2), 6.30 (m, 2H, CH═CH−CH_3). ^{13}C NMR (DMSO-d_6) δ 18.6, 43.9, 44.5, 56.6, 59.3, 70.4, 78.8, 83.3, 86.6, 122.2, 129.9, 131.4. HR-MS: m/z found (calcd) 345.0276 (345.0302) {[M − PF_6^-]$^+$ = [$C_{12}H_{20}N_2ORuCl$]$^+$}. Anal. Calc. for $C_{12}H_{20}N_2ORuClPF_6$●CH_3OH: C, 29.92%; H, 4.64%; N, 5.37%. Found: C, 29.59%; H, 4.51%; N, 5.53%.

2.3.4. Synthesis of [Ru(η^6-2-(1-propenyl)anisole)(en)I]PF_6 (**4**)

The procedure described above for compound **3** was used for 118 mg of [Ru(η^6-2-(1-propenyl)anisole)$_2$$I_2$]$_2$ (0.12 mmol), 28 μL of ethylenediamine (0.42 mmol), and 100 mg of NH_4PF_6 (0.61 mmol). The product was recrystallized in a mixture of MeOH-ether, enabling the isolation of 33 mg of product (0.057 mmol, 24% yield). ^{1}H NMR (DMSO-d_6) δ 1.80 (d, J = 4.2 Hz, 3H, CH═CH−CH_3), 2.18 (m, 1H, N−CH_2−CH_2−N), 2.32 (m, 2H, N−CH_2−CH_2−N), 3.83 (s, 3H, OCH_3), 4.13 (m, 1H, H_2N−C−C−NH_2), 4.45 (m, 1H, H_2N−C−C−NH_2), 5.30 (m, 1H, Ar-H), 5.47 (d, J = 4.8 Hz, 1H, Ar-H), 5.94 (m, 1H, Ar-H), 6.00 (m, 1H, H_2N−C−C−NH_2), 6.15 (m, 2H, Ar-H; H_2N−C−C−NH_2), 6.35 (m, 2H, CH═CH−CH_3). ^{13}C NMR (DMSO-d_6) δ 18.6, 44.3, 45.1, 56.7, 59.4, 72.5, 79.4, 83.5, 86.4, 122.5, 130.7, 131.6. HR-MS: m/z found (calcd) 436.9629 (436.9658) {[M − PF_6^-]$^+$ = [$C_{12}H_{20}N_2ORuI$]$^+$}. Anal. Calc. for $C_{12}H_{20}N_2ORuIPF_6$●CH_3OH: C, 25.46%; H, 3.94%; N, 4.57%. Found: C, 25.18%; H, 4.00%; N, 4.59%.

2.4. Lipophilicity analysis

The lipophilicity was determined using the shake flask method [21] and the results were expressed as distribution coefficient (Log D [Ru-X]) values. The shake flask experiments were carried out at 25 °C in triplicate for each compound. In a 50 mL bottle, 5 mL of octanol saturated with 0.2 M HCl were added to 5 mL of the aqueous solution saturated with octanol containing the ruthenium compounds (approximately 2.5 mg). The bottle with both phases was shaken in a vortex system for 2 h and then centrifuged at 3000 rpm for 10 min. It was then allowed to stand for 24 h, followed by the separation of the phases. The amount of ruthenium compounds in the aqueous phase was determined by measuring the atomic absorption (n = 4).

2.5. Atomic absorption method

An Agilent Technologies AA 240 flame atomic absorption spectrometer equipped with hollow cathode lamps was used for the analyses. The instrumental parameters were adjusted according to the manufacturer's recommendations. For the analysis, a Ru hollow cathode lamp with a current of 6.0 mA operating at 349.9 nm was used. The flame composition was N_2O-acetylene (11−50 psi).

The aqueous phase was digested on a heating plate (70−75 °C) using a mixture of 3 mL of HNO_3/HCl (3:1 v/v). After cooling, the residue was transferred to 10 mL volumetric flasks, and 0.433 g of $La(NO_3)_3$•$6H_2O$ and 0.67 mL of HCl were added and then diluted to level with deionized water. Prior to the analysis, the samples were filtered through a 0.45 μm membrane filter. The samples were analyzed in quintuplicate.

2.6. Kinetic measurements

A UV−Vis Thermo Scientific Evolution 220 spectrophotometer equipped with a Thermo Scientific SPE-8W thermostat was utilized for the kinetic measurements. Aliquots of 0.15 mL of 1 mM stock solutions of compounds **1**–**4** and [Ru(η^6-*p*-cymene)(en)I]PF_6 in MeOH were diluted in 2.85 mL of H_2O (Milli-Q) and the UV−Vis spectra were recorded at 298 K between 200 and 500 nm at 30 s (t_0), 50 s, and 2, 4, 6, 10, 15, 20, 25, 30 and 35 min. The time evolution of UV−Vis difference spectra for the aquation process allowed us to identify the wavelength to be employed for the kinetic studies. The hydrolysis rate constant (k_{H2O}) was determined at intervals of 5 s using the same conditions described above, and the data were processed using OriginPro 8 software.

2.7. Calculation studies

All calculations were performed using DFT implemented in ORCA 4.0.1.2. In our *in silico* investigation, we used the non-truncated models of the complexes investigated experimentally. Final geometry optimizations were performed using the hybrid-meta GGA TPSSh [22] function in combination with the def2-SV(P) basis set [23], the def2/J auxiliary basis [24] and the Def2-ECP relativistic core potentials for Ru and I [25]. We applied the RI [26] and RIJCOSX [27] approximations and used GridX4 and Grid4 to accelerate the geometry optimizations. Dispersion was considered in all calculations, including geometry optimizations, using Grimme's D3 method [28] in combination with the Becke-Johnson damping scheme [29], which is often denoted as D3BJ. Numerical vibrational frequency calculations were conducted at the same level of theory using central difference approximation with a 0.001 increment to confirm that the optimized structures correspond to either minima or first-order saddle points (transition state) of the potential energy surface and to obtain thermodynamic corrections for the electronic energy within the ideal gas−rigid rotor−harmonic oscillator approximation at T = 273.15 K. The energies of the optimized structures were reevaluated using the triple-ζ basis set def2-TZVP (Def2-ECP still applies for Ru and I) [23] using Grid5 and D3BJ, without approximating the integrals with RI or RIJCOSX.

Solvation energies with water as the solvent were also computed with the latter method, approximations and grid using the SMD implicit solvation model [30]. We used the default method to create the molecular surface of the solute-solvent boundary, and

we adjusted the atomic radii used to generate the solute surface to the following values: H (1.150 Å), C (1.900 Å), N (1.600 Å), O (1.600 Å), Cl (1.974 Å), I (2.250 Å), and Ru (1.481 Å) while the radius of solvent (water) was set to 1.40 Å. In this context, the computation of the solvation energy, ΔG^{solv}, of small charged ions, such as I^- and Cl^- in our study, is generally challenging [31]. Accordingly, when evaluating the stability of products and intermediates with extruded free halide ions, we used ΔG^{solv} values of −59.9 kcal mol^{-1} and -74.6 kcal mol^{-1} for bare I^- and Cl^-, respectively, which were derived from experimental Gibbs free energy of hydration [31] and consistent with a previous compilation of experimental values [32]. Finally, we adopted the protocol described by Wertz to account for the entropy change of species when going from the gas phase (1 atm) to aqueous solution (1 M) [33], which separates the solvation entropies, ΔS_{sol}, into three steps: (i) compression of the gas phase solute from 1 atm to $V_{m,liq}$, (ii) a transition from the gas at its liquid-phase density to liquid, resulting in a significant loss of entropy, and (iii) expansion of the solute from $V_{m,liq}$ to the corresponding volume based on the density of the solution. Based on this concept, Cooper and Ziegler [34] derived the expression of $\Delta S^{solv} = -0.26 - 0.46 S_{gas}$ cal·mol^{-1} K^{-1} for the change in the entropy of the state change of water, where S_{gas} is the gas phase entropy of a particular species. We used this equation to derive the final entropy contributions in the aqueous solution state for all calculated species, except for I^- and Cl^-, for which we used experimental Gibbs free energies of solvation, ΔG^{solv}, including ΔS^{solv}.

2.8. Cell lines

The human GC cell line AGS (ATCC® CRL-1739™) was cultured in Ham's F−12K (Kaighn's) culture medium (Corning), while the human GC cell line SNU1 (ATCC® CRL5971™) was cultured in RPMI 1640 culture medium. GES-1 normal human gastric epithelial cells were used as a control (kindly donated by Dr. Dawit Kidane-Mulat from the University of Texas at Austin), and cultivated in DMEM (Corning). The media were supplemented with 10% FBS, 100 units/mL penicillin G, and 100 μg/mL streptomycin. All cell types were incubated at 37 °C with a 5% CO_2 atmosphere in a humidified incubator.

2.9. Cell viability: in vitro growth inhibition assay

Cells were seeded in 96-well plates at a density of 5,000 cells/well in their respective culture medium and incubated for 24 h. Thereafter, the cells were treated with different concentrations of ruthenium compounds (0.78, 1.5, 3.1, 6.25, 12.5, 25, 50, and 100 μM) for additional 24 h. Then the cell viability was determined using the MTS reduction assay by first adding 20 μL of CellTiter 96® AQueous One Solution Cell Proliferation Assay System (Promega) to each well and then incubating the plate for 2 h. Stock solutions of the complexes were prepared in DMSO, and the concentration of DMSO was maintained at 0.1% in all experiments. Absorbance measurements were recorded using a NOVOstar 700-0130 at 490 nm. Cisplatin treatment was used as a control. The experiments were performed in 6 replicates for each drug concentration and were carried out three times independently.

Cellular viability was calculated as follows:

$$\%Cell\ \ viability = \frac{OD\ \ treatment}{OD\ \ control} x\ \ 100$$

The formula used to calculate IC_{50} was

$$Y = 100 / (1 + 10\text{^}((LogIC_{50}\text{-}X) * Hill\ Slope))$$

where X = log of the concentration; Y = normalized response; Hill Slope: slope factor.

2.10. Cell viability: statistical analysis

IC_{50} values were calculated as mean ± standard error of three measurements. Statistical comparisons were performed using ANOVA and the non-parametric Kruskal-Wallis test followed by Dunn's multiple comparison test. P-values less than 0.05 ($p < 0.05$) were considered significant.

3. Results and discussion

3.1. Synthesis and characterization of compounds 3 and 4

Scheme 1 summarizes the experimental procedure for the synthesis of dimeric compounds (**5** to **8**) and the target monometallic species (**1** to **4**). The experimental conditions employed for the synthesis of $[Ru(\eta^6\text{-arene})_2Cl_2]_2$, where arene: 4-(1-propenyl) anisole or anethole (**5**) and 2-(1-propenyl)anisole (**6**), were slightly modified compared to procedure that we developed in our previous study [11]. The polymeric ruthenium precursor $[Ru(\eta^4\text{-}1,5\text{-}COD)Cl_2]_n$ was reacted with the neat ligand (4-allylanisole or 2-allylanisole) at 100−110 °C, isolating the desired dimeric compounds with similar yields. Despite the lack of improvement in the reaction yield, the time required to complete the first two steps (Scheme 1) was optimized to some extent. The iodide dimeric analogues $[Ru(\eta^6\text{-arene})I_2]_2$ (**7** and **8**) were obtained using established conditions at 76% and 54% yields, respectively. The four organometallic compounds $[Ru(\eta^6\text{-arene})(en)X]PF_6$ (**1** to **4**) were finally obtained as PF_6^- salts using the established method. After recrystallization of all of these complexes through the slow diffusion of ether into MeOH solution, suitable crystals of compounds **1** and **3** were collected for X-ray diffraction studies. Although the synthesis of compound **1** has been already reported by our research group, its crystallographic characterization was still pending.

Here, we report the structures of $[Ru(\eta^6\text{-}4\text{-}(1\text{-propenyl})anisole)(en)Cl]^+$ (**1**) and $[Ru(\eta^6\text{-}2\text{-}(1\text{-propenyl})anisole)(en)Cl]^+$ (**3**) with PF_6^- as a counter ion obtained using single crystal X-ray diffraction (Fig. 2). In both compounds, one aromatic ring, two nitrogen atoms of the chelating en (ethylenediamine) ligand and a chloride ion coordinate the ruthenium(II) center, forming a pseudo-octahedral overall geometry. The relevant structural parameters, such as bond distances and angles, are provided in Table 2, and are consistent with the values published for $[Ru(\eta^6\text{-anethole})(en)Br]PF_6$ [13] and the values observed for the analogous compounds with *p*-cymene and biphenyl as arene ligands [3]. Notably, however, the alkyl groups of C8, C9, and C10 are tilted out of the mean plane of aromatic groups with a C3−C2−C8−C9 torsion angle (at C2: C8−C9−C10) of 35.0(7)° in compound **1**, and a torsion angle C3−C4−C8−C9 (at C4: C8−C9−C10) of −20.6(14)° in compound **3**. The C8−C9 (Csp^2-Csp^2) bond distance of 1.311(8) Å and C8−C9−C10 angle of 126.4(6)° in compound **1** and 1.322(13) Å and C8−C9−C10 = 126.7(9)° in compound **3**, respectively, are similar to the values observed for the $[Ru(\eta^6\text{-anethole})(en)Br]PF_6$ analogue. The methoxy group is essentially in the mean plane of aromatic ring (see Table 2). The N−Ru−N bond angles in compounds **1** and **3** also closely resemble $[Ru(\eta^6\text{-anethole})(en)Br]PF_6$. The largest structural difference between compounds **1** and **3** is in the en ligand displaying N1−C11−C12−N2 torsion angles of 19.1(10)° and −55.9(8)°, respectively, displaying differences similar to eclipsed and staggered arrangements along the N−C−C−N chain. An analysis of the crystal structure at the supramolecular level reveals that in addition to electrostatic interactions, hydrogen bonds also play a role in maintaining the structure of the cationic

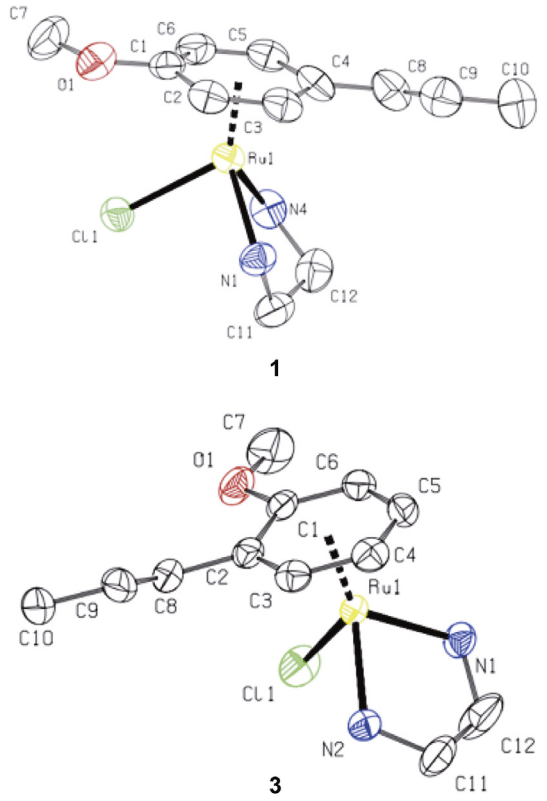

Fig. 2. X-ray structures of compound **1** and **3**. Displacement ellipsoids are drawn at the 30% probability level. PF_6^- anions and H atoms have been omitted for clarity.

complexes and PF_6^- counter ions. In compound **3**, for example, the hydrogen atoms of the NH_2 functionalities of the en ligand develop hydrogen bonds with each fluorine atom, forming a graph-set $C_2^2(4)$ descriptor motif (Fig. S7, Supplementary Material) [35], while similar hydrogens form secondary interactions with fluorine and chlorine in compound **1**, producing graph-set $C_1^2(7)$ and $R_2^2(4)$ descriptor motifs, respectively (Fig. S6, Supplementary Material). Moreover, weak interactions involving the aromatic C–H group of the anisole ring and fluorine atoms at distances of 2.46–2.52 Å were also clearly observed in the crystal packing of both molecules.

Further characterization of compounds **3** and **4** using ^1H and ^{13}C NMR spectroscopy confirmed the bonding pattern that was revealed in the X-ray structure in solution state. Fig. 3 shows the chemical shifts of the aromatic protons of the free and coordinated 2-(1-propenyl)anisole ligand in compound **3**. The four aromatic signals at δ 7.40 ppm (d, $J = 7.5$ Hz, 1H, H-6), 7.17 (dd, $J = 7.8$, 7.8 Hz, 1H, H-5), 6.94 (d, $J = 8.2$ Hz, 1H, H-3) and 6.88 (dd, $J = 7.5$, 7.5 Hz, 1H, H-4) experienced a significant upfield shift (approximately 1.5 ppm) in the organometallic compound. These shifts are similar to those observed in the previously reported compounds [Ru(η^6-anethole)(en)Cl]PF_6 and [Ru(η^6-methylisoeugenol)(en)Cl]PF_6 [11], and are characteristic features of organometallic bond formation in these species (Fig. S8, Supplementary Material) [36]. Consistent with this finding, the carbon signals associated with the aromatic ring underwent a characteristic upfield shift between 20 and 50 ppm upon forming the ruthenium(II)-arene interaction in compound **3** (Fig. S9, Supplementary Material).

3.2. Lipophilicity measurements

The experimental determination of the lipophilicity of compounds **3** and **4** was performed using a validated procedure that has been adapted and repeatedly used by our research group [14]. A direct comparison of the distribution coefficient data (Log *D* [Ru-X], Table 4) obtained from compound **3** with compound **1** did not reveal a significant effect of the change of the position of the 1-propenyl chain from the *para* (for anethole) to *ortho* position in the coordinated arene on this physicochemical property of the studied organometallic compounds. When measuring the lipophilicity of compound **4**, we obtained a value (Log *D* [Ru-X]: -1.18 ± 0.06) that is not different, i.e., within the range of error, from compound **3**. This finding is somewhat puzzling, given the recorded differences in lipophilicity for complexes **1** and **2**, and for other compounds, such as aminoflavone and aminochromone Ru(II) compounds [37]. This indistinguishable lipophilic behavior of compounds **4** and **3** is attributed to the low aqueous stability of compound **4** in chloride media (0.2 M HCl), leading to iodido-chlorido exchange at the onset of the measurement. Evidence for this exchange process was collected using ^1H NMR spectroscopy by monitoring the stability of compound **4** in an aqueous 0.2 M HCl solution, revealing an almost complete conversion of compound **4** to compound **3** under these conditions after 24 h (Fig. S10, Supplementary Material). The analogous conversion of compound **2** to compound **1** was also detected under the same conditions; however, the extent of exchange is partial, manifesting therefore in distinguishable Log *D* [Ru-X] values amongst these compounds.

Table 2
Selected bond lengths (Å) and angles (°) in [Ru(η^6-4-(1-propenyl)anisole)(en)Cl]$^+$ (**1**) and [Ru(η^6-2-(1-propenyl)anisole)(en)Cl]$^+$ (**3**). Values in square brackets correspond to equilibrium structures computed at the TPSSh/def2-SVP level of theory.

	(1)	(3)
Ru···*Cg*[a]	1.680(3)	1.6759(4)
Ru–Cl	2.4152(18) [2.386]	2.3899(16) [2.389]
Ru–N1	2.128(7) [2.137]	2.127(4) [2.154]
Ru–N2	2.145(7) [2.152]	2.127(4) [2.136]
C1–O1	1.372(9) [1.320]	1.3408(2) [1.323]
N1–Ru–N2	78.7(3) [79.3]	79.22(14) [79.56]
N1–Ru–Cl	85.6(2) [81.90]	84.33(11) [81.42]
N2–Ru–Cl	84.70(19) [82.14]	84.62(11) [82.09]
C1–C2–C3	119.5(7) [119.48]	119.4(4) [117.52]
C6–C1–O1–C7	8.773(3) [7.18]	8.787(1) [6.12]

[a] *Cg* represents the centroid of the C1–C6 ring.

3.3. Kinetic measurements

The hydrolysis of complexes with the general formula of [Ru(η^6-arene)(en)X]$^+$, where X is the leaving halide group, to the corresponding aqueous metabolite [Ru(η^6-arene)(en)(H_2O)]$^{+2}$ is a key feature of this type of species, as it is commonly correlated with the *in vitro* cytotoxic activity of the organometallic complex [38,39]. ^1H NMR spectra revealed the appearance of additional signals associated to the aquo-Ru(II) metabolite formed as a consequence of the hydrolysis of compound **3** and **4** (after 24 h). The addition of sodium chloride to the hydrolysis mixture of compound **3** (to achieve a 100 mM concentration within the NMR test tube) restores its original spectrum (Fig. S11, Supplementary Material) such as was reported for compound **1** [13]. The kinetics of hydrolysis were examined using 50 μM aqueous solution of compounds **1** to **4**, and the time dependence of the UV–Vis absorption spectra of the process were monitored for 30–80 min at 298 K. Fig. 4 shows the Δ absorbance over time (35 min) between 200 and 500 nm for compound **1**, which was determined to establish the maximum change in absorbance for further kinetic studies (Figs. S12–S14, Supplementary Material for data from compounds **2**, **3** and **4**).

Table 3 summarizes the rates of the pseudo-first order hydrolysis process (expressed as k_{H2O} 10^{-3} s^{-1}) for the four (1-propenyl)

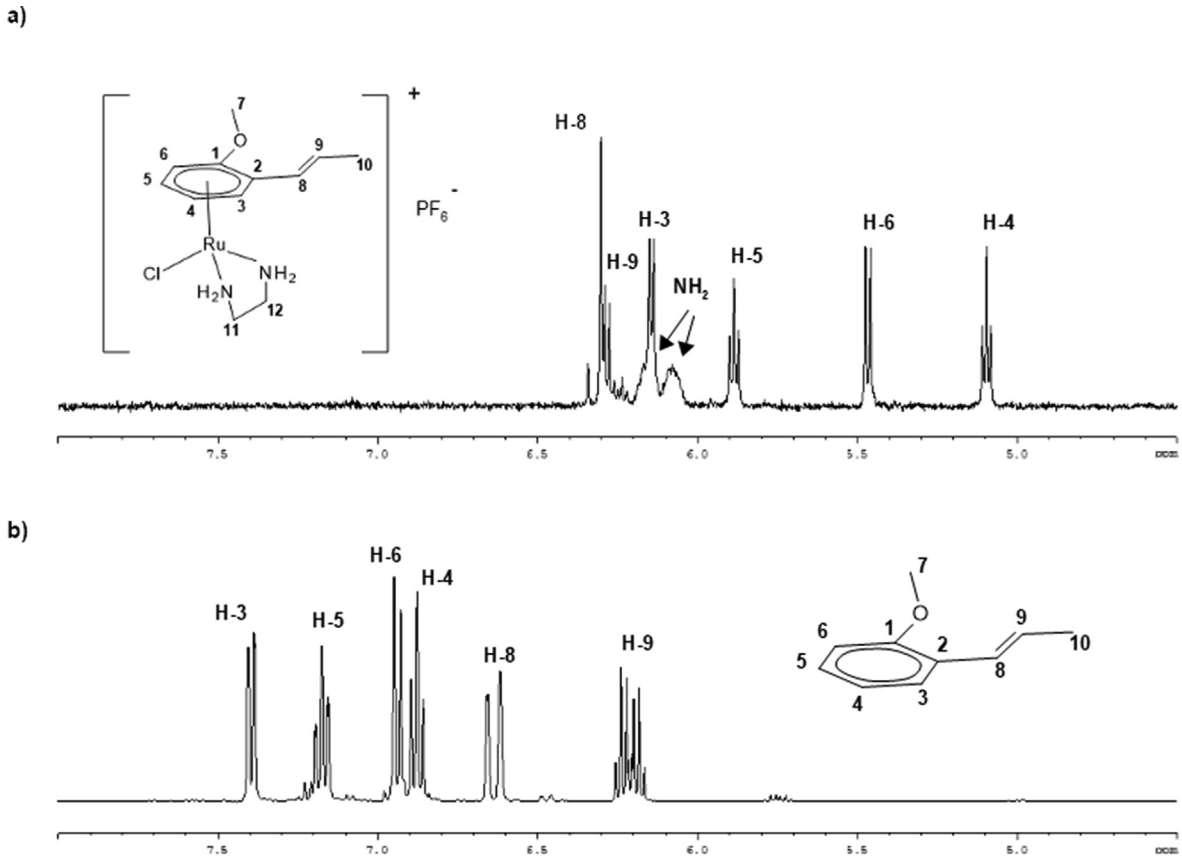

Fig. 3. ^{1}H NMR spectra of compound **3** (a) and free 2-(1-propenyl)anisole (b).

anisole complexes **1** to **4**. The exchange of the chloride leaving group for iodide in either the Ru(η^6-2-(1-propenyl)anisole)(en) or in the Ru(η^6-4-(1-propenyl)anisole)(en) scaffold slows the hydrolysis rate by approximately one order of magnitude. This finding supports the previously observed trend for other [Ru(η^6-arene)(en)X]$^+$ compounds, where X = Cl or I, which are also indicated in parenthesis in Table 3. Consistent with the aforementioned results for lipophilicity, the change in the substitution pattern from the *para* to *ortho* position of the 1-propenyl chain of the arene ligand does not exert a significant effect on the hydrolysis rate of these compounds. We extended our kinetic analysis to the parent [Ru(η^6-*p*-cymene)(en)I]$^+$ species with available experimental data and we

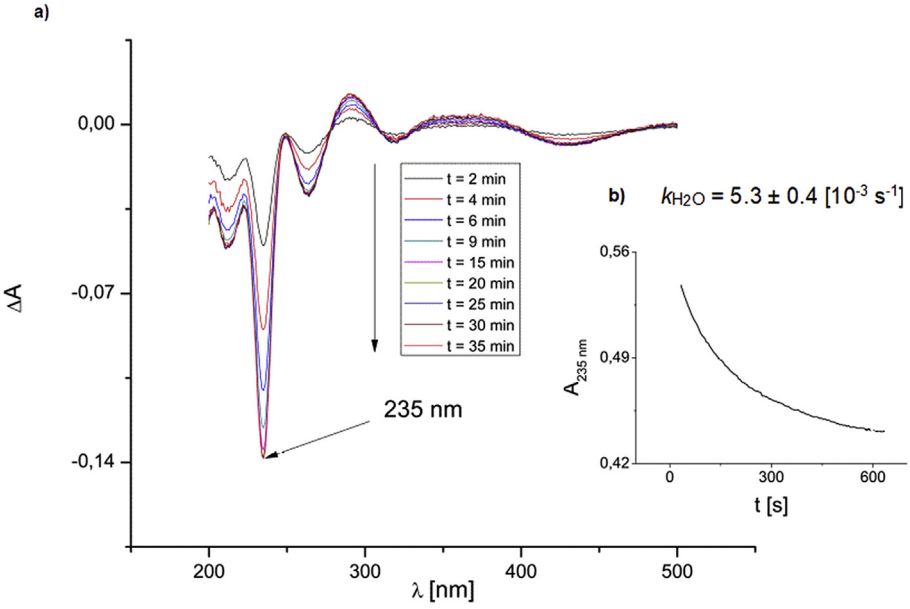

Fig. 4. a) Change in absorbance (express as Δ*A*) upon hydrolysis in the range 200–500 nm for compound **1** at 298 K; b) first-order exponential decay of the absorbance of compound **1** at 235 nm.

Table 3
Hydrolysis rate constants of compounds **1** to **4** and other relevant [Ru(η^6-arene)(en)X]PF_6 compounds at 298 K.

Compound	k_{H2O} [10^{-3} s^{-1}] (298 K)	
	X = Cl	X = I
[Ru(η^6-2-(1-propenyl)anisole)(en)X]PF_6	4.1 ± 0.2	0.76 ± 0.03
[Ru(η^6-4-(1-propenyl)anisole)(en)X]PF_6	5.3 ± 0.4	0.56 ± 0.01
[Ru(η^6-*p*-cymene)(en)X]PF_6	–	0.58 ± 0.01 (0.948 ± 0.008) [b]
[Ru(η^6-benzene)(en)X]PF_6	(1.98 ± 0.02) [b]	(0.294 ± 0.003) [b]
[Ru(η^6-biphenyl)(en)X]PF_6	(1.23 ± 0.01) [a]	(0.321 ± 0.045) [b]

[a] Ref [38].
[b] Ref [40].

measured its kinetic rate constant under our experimental conditions using our procedure to assess the consistency of our kinetic measurements to previously reported data. A comparison of these two experimental datasets suggests that a normalization factor of approximately 1.6 is needed to ensure that two sets of experimental data are equivalent. The rate constants listed in Table 3 imply that the coordination of (1-propenyl)anisole (in the *para* or *ortho* position) to the Ru(en) moiety generates organometallic compounds that are as active as those complexes that employ *p*-cymene as the arene ligand.

3.4. Computational studies

We used density functional theory (DFT) coupled with implicit solvation and computed the most plausible reaction pathways using an established computational protocol to obtain molecular level insights into the mechanism of hydrolysis of compounds **1** to **4**. We performed this *in silico* investigation using models of the experimentally studied complexes without any truncation at the TPSSh-D3/Def2-TZVP (crossref TPSSh and daf2 basis sets) level of theory using ORCA. Consistent with the findings and conclusions of earlier studies [41], we also repeatedly confirmed [42,43] that the meta-GGA hybrid TPSSh function in combination with Grimme's D3 dispersion correction and a flexible basis set provides reliable descriptions of various properties of transition metal complexes, including the equilibrium geometry, redox potential, electronic structure, reactivity and even spin-state energetics. Together with these benchmarks, the agreement between computed and experimental molecular structures reported in Table 2 convincingly implies that our computer models capture the most salient features of these molecular systems reasonably well and that the utilized approximations are acceptable. Thus, a detailed analysis of the structure, bonding pattern and stability of complexes is justified and promises to reveal relevant aspects of the mechanism of hydrolysis of ruthenium-(1-propenyl)anisole derivatives.

The considered reaction pathways are illustrated in Fig. 5 and comprise dissociation-initiated and direct interchange ligand substitutions for the four complexes, **1** to **4**. As shown in Fig. 5, the interchange mechanism for the replacement of halides with water is a generally low energy channel that is the most plausible mechanism of hydrolysis for all the studied derivatives. The key feature of this interchange mechanism is the simultaneous entrance of a water molecule and departure of the halide ligand, leading to the formation of the water-ligated products **1(H_2O)**, **2(H_2O)**, **3(H_2O)** and **4(H_2O)**. This ligand substitution process occurs in one elementary step traversing a central transition state, for example, $\mathbf{TS^{3+H2O}}$ for compound **3**, as displayed in Fig. 5. Although complexes **1** to **4** are formally octahedral, leading to the formation of seven-coordinated transition state structures upon associative interchange, these TS structures are not critically congested due to the small binding angle of the arene ring to the ruthenium center. This hypothesis is clearly confirmed in the representative transition state structure $\mathbf{TS^{3+H2O}}$ shown in Fig. 5. The calculated activation barriers vary in a very narrow range from 10.8 to 11.6 kcal mol^{-1}. Accordingly, we attribute these balanced energy landscapes and facile interchange-based ligand exchange processes to the non-congested transition state geometries and to the electrostatic stabilization effect of the halide ion that is located in relatively close proximity to the formal Ru(II) center during the bond breaking-forming process. Finally, our experimental findings unambiguously confirm that the hydrolysis rate is approximately 5–10 times faster for the chloride than for the iodide derivatives, which translates into a ~1 kcal mol^{-1} difference in activation barriers. Although the studied systems are highly similar, considerably reducing the relative methodical error, the innate approximations of DFT and implicit solvation do not allow the realistic differentiation of the computed activation barriers to the resolution of the experimental data. Based on these limitations of the *in silico* method, the computed barriers imply similar reaction rates for the hydrolysis of compounds **1** to **4**. The same conclusion was drawn for the calculations of the relative stability of chloride and iodide complexes. If evaluated based on the halide exchange reactions, $\mathbf{1} + I^- \rightarrow \mathbf{2} + Cl^-$ and $\mathbf{3} + I^- \rightarrow \mathbf{4} + Cl^-$, the iodide complexes (**2** and **4**) are computed to be more stable by 0.2 and 0.3 kcal mol^{-1} than

Table 4
Lipophilicity (Log *D* $[Ru\text{-}X]_{org}/[Ru\text{-}X]_{ac}$) and anti-proliferative activity (expressed as IC_{50} values) of compounds **1** to **4** toward the gastric cancer cell lines AGS and SNU-1, and the normal gastric cell line GES-1. [Ru(η^6-*p*-cymene)(en)X]PF_6 (X: Cl, I) and cisplatin were included as controls.

Compound	Log *D* [Ru-X]	IC_{50} ± SE (μM)		
		AGS	SNU-1	GES-1
3	−1.2 ± 0.1	82.6 ± 1.12	8.27 ± 1.10	150.20 ± 1.35
4	n. incl.	n. incl.	n. incl.	n. incl.
1	−1.39 ± 0.04 [a]	71.71 ± 1.86 [a]	7.62 ± 1.13	75.94 ± 1.12
2	−1.00 ± 0.02 [a]	11.27 ± 1.08 [a]	–	50.93 ± 1.69 [a]
[Ru(η^6-*p*-cymene)(en)Cl]PF_6	–	108.30 ± 1.21	28.00 ± 1.07	67.17 ± 1.21
[Ru(η^6-*p*-cymene)(en)I]PF_6	–	149.30 ± 1.46	15.48 ± 1.06	72.49 ± 1.06
cisplatin	–	32.50 ± 3.50	57.93 ± 1.08	22.34 ± 1.11

n. incl.: not included.
[a] Ref [14].

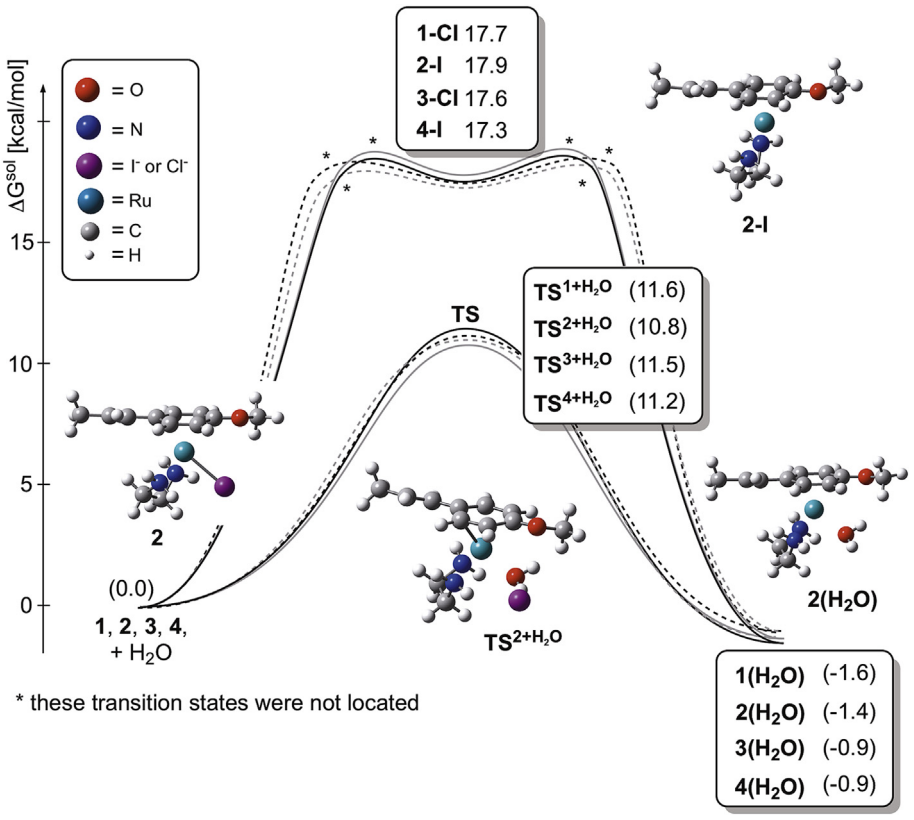

Fig. 5. Solution-state Gibbs free energy profile of associative interchange and dissociative pathways of the hydrolysis of complexes **1** to **4**.

the chloride derivatives (**1** and **3**), and this difference implies very similar thermodynamic stabilities.

The onset of the dissociative mechanisms is halide (Cl^- or I^-) departure from the corresponding reactant to form a coordinately unsaturated intermediate (**1-Cl**, **2-I**, **3-Cl** and **4-I**) with a relative solution state stability of approximately 17.5 kcal mol^{-1}. As the preceding halide dissociation and succeeding water association steps appear to be barrierless processes on the potential energy surfaces, these pathways are also viable at room temperature and, accordingly, dissociative hydrolysis of compounds **1**–**4** is kinetically allowed. Nevertheless, this mechanism has no practical relevance, as the interchange mechanism discussed above occurs approximately 10^6-fold faster at room temperature based on the scrutinized pathways. Accordingly, computations directly support the experimental findings of Sadler and co-workers on the kinetics of aquation and anation of ruthenium(II) anticancer complexes, including RM175 (Fig. 1) and its derivatives, revealing activation parameters (for example, negative $\Delta S^{\ddagger}$ values) that are characteristic of associative interchange (I_a) mechanisms [38].

3.5. In vitro cell viability assay

The anti-proliferative activity of the new ruthenium compounds (3 and 4) toward the human gastric cancer cell lines AGS and SNU-1 and normal gastric cell line GES-1 was measured after 24 h using an MTS assay. The results were compared to findings already reported for compounds 1 and 2, Ru(II)-*p*-cymene derivatives, and cisplatin. Based on the IC_{50} values, which are summarized in Table 4, all ruthenium compounds inhibited cell proliferation in a dose-dependent manner.

These IC_{50} values show that compound **3** exhibits a biological activity toward the gastric cancer cell line AGS that is very similar to the previously reported isomer **1**, which is expected to a large extent due to the similarities in lipophilicities and hydrolysis kinetics. Consistent with the discussions above, due to its conversion to compound **3** in presence of chloride anions, the IC_{50} values for compound **4** are not reported in Table 4. Indeed, the assessed IC_{50} values for compound **4** (IC_{50} = 81.13 ± 1.10 μM toward AGS cells, IC_{50} = 9.05 ± 1.11 μM toward SNU-1 cells and IC_{50} = 111.40 ± 1.09 μM toward GES-1 cells) may actually reflect the cytotoxicity of the chloride analogue **3** that could form *in situ* during the biological evaluation (24 h). The cell culture medium, which is rich in chloride salts, provides the appropriate conditions for this process to occur and might obscure the determination of the activity of the parent compound.

On the other hand, the synthesized compound **3**, together with the previously prepared compounds **1** and **2**, exhibited a slight increase in cytotoxicity compared to the lead compounds [Ru(η^6-*p*-cymene)(en)X]PF_6 (X: Cl and I) against both gastric cancer cell lines (AGS and SNU-1), which prompted us to further explore the activities of structurally related compounds toward these cancer cell lines. The IC_{50} values revealed that the ruthenium compounds generally exhibited a better biological activity toward the SNU-1 tumor cell line than the AGS cell line, and the selectivity between SNU-1 and GES-1 cells (tumor versus non tumor cells) was greater than the commercial drug cisplatin, one drug employed in the therapeutic regime for gastric cancer. The potential application of ruthenium compounds in this field of research deserves further study in the future.

4. Conclusions

In this study, we presented the synthesis and complete characterization of two new derivatives of the [Ru(η^6-arene)(en)Cl]PF_6

family, namely, compounds **3** and **4**, produced using the same synthetic strategy as the previously reported structural isomers **1** and **2**. Our experiments also analyzed the lipophilicity and hydrolysis rate constants of compounds **1** to **4**, revealing that the change in the substitution pattern of the coordinated arene from 4-(1-propenyl)anisole (or anethole) to 2-(1-propenyl)anisole exerted a subtle effect on these properties. The kinetic experiments revealed that compounds **1** to **4** exhibited hydrolysis reactions rates that were approximately as fast as some of the lead compounds that contain *p*-cymene as the arene ligand. According to the computational study, the interchange mechanism governs the hydrolysis process of the four compounds studied, and no significant difference was observed between the energies of the transition state. Hence, a direct agreement between the theoretical and experimental studies could be observed. The *in vitro* anti-proliferative activity of compounds **1** to **3** generally revealed better cytotoxicity and selectivity (tumor versus non tumor) toward the gastric tumor cell lines studied than the $[Ru(\eta^6\text{-}p\text{-cymene})(en)X]PF_6$ (X: Cl, I) compounds. However, compound **3** does not show enhanced biological behavior compared to the previously reported isomers **1** and **2**, as the latter remain as the most promising compounds to target these human gastric tumor cell lines. Finally, because the studied arene ligand 4-(1-propenyl)anisole (or anethole) led us to biologically active ruthenium compounds, the challenge of designing novel compounds by optimizing the kinetics of hydrolysis may facilitate the development of more active complexes.

Declaration of competing interest

The authors declare that they have no known competing financial interests or personal relationships that could have appeared to influence the work reported in this paper.

Acknowledgments

The authors are thankful to the Universidad Técnica Federico Santa María (DGIIP 116.13.1) and CORFO (14IDL2-30087) for providing the financial support. Dr. Giuliano Bernal thanks Dr. Dawit Kidane-Mulat for kindly donating the GES-1 cells used in this study. Dr. Balazs Pinter also wishes to acknowledge CCTVal for the computational resources and technical assistance provided for implementing the DFT study.

Appendix A. Supplementary data

Supplementary data to this article can be found online at https://doi.org/10.1016/j.jorganchem.2019.121094.

Supplementary Material.

The supplementary material related to this article can be found on the web free of charge.

References

[1] R. Trondl, P. Heffeter, C. Kowol, M. Jacupec, W. Berger, B.K. Keppler, Chem. Sci. 5 (2014) 2925–2932.
[2] A. Bergamo, G. Sava, Chem. Soc. Rev. (2015) 8818–8835.
[3] R. Morris, R. Aird, S. Murdoch, H. Chen, J. Cummings, N. Hughes, S. Parsons, A. Parkin, G. Boyd, D. Jodrell, P.J. Sadler, J. Med. Chem. 44 (2001) 3616–3621.
[4] C.S. Allardyce, P.J. Dyson, D.J. Ellis, S.L. Heath, Chem. Commun. 2 (2001) 1396–1397.
[5] A. Nazarov, C. Hartinger, P.J. Dyson, J. Organomet. Chem. 751 (2014) 251–260.
[6] S. Dougan, P.J. Sadler, Chim. Int. J. Chem. 61 (2007) 704–715.
[7] R. Pettinari, F. Marchetti, F. Condello, C. Pettinari, G. Lupidi, R. Scopelliti, S. Mukhopadhyay, T. Riedel, P.J. Dyson, Organometallics 33 (2014) 3709–3715.
[8] M. Babak, D. Plazuk, S. Meier, H. Arabshahi, J. Reynisson, B. Rychlik, A. Blauz, K. Szulc, M. Hanif, S. Strobl, A. Roller, B.K. Keppler, C. Hartinger, Chem. Eur J. 21 (2015) 5110–5117.
[9] A. Kurzwernhart, S. Mokesch, E. Klapproth, M. Adib-ravazi, M. Jakupec, C. Hartinger, W. Kandioller, B.K. Keppler, Eur. J. Inorg. Chem. (2016) 240–246.
[10] R. Pettinari, A. Petrini, F. Marchetti, C. Pettinari, T. Riedel, B. Therrien, P.J. Dyson, Eur. J. Inorg. Chem. (2017) 1800–1806.
[11] R. Delgado, A. Galdamez, J. Villena, P.G. Reveco, F.A. Thomet, J. Organomet. Chem. 782 (2015) 131–137.
[12] A. Habtemariam, M. Melchart, R. Fernández, S. Parsons, I. Oswald, A. Parkin, F. Fabbiani, J. Davidson, A. Dawson, R. Aird, D. Jodrell, P.J. Sadler, J. Med. Chem. 49 (2006) 6858–6868.
[13] D. Astudillo, A. Galdamez, M.E. Sanguinetti, J. Villena, F.A. Thomet, Inorg. Chem. Commun. 84 (2017) 221–224.
[14] E. Carrillo, S. Ramírez-Rivera, G. Bernal, G. Aquea, C. Tessini, F.A. Thomet, Life Sci. 217 (2019) 193–201.
[15] M.O. Albers, T.V. Ashworth, H.E. Oosthuizen, E. Singleton, Inorg. Synth. (1987) 68–77.
[16] Bruker Analytical X-ray Instruments, SMART, SAINTPLUS V6.02, SHELXTL V6.10 and SADABS, (n.d.).
[17] G.M. Sheldrick, Acta Crystallogr. Sect. C Struct. Chem. 71 (2015) 3–8.
[18] O.V. Dolomanov, L.J. Bourhis, R.J. Gildea, J. Howard, H. Puschmann, J. Appl. Crystallogr. 42 (2009) 339–341.
[19] K. Brandenburg, DIAMOND, Visual Crystal Structure Information System, 1e Crystal Impact GbR, 1999. Version 2.
[20] A.L. Spek, J. Appl. Crystallogr. 36 (2003) 7–13.
[21] Y. Qiao, S. Xia, P. Ma, J. Chem. Eng. Data 53 (2008) 280–282.
[22] J. Tao, J.P. Perdew, V.N. Staroverov, G.E. Scuseria, Phys. Rev. Lett. 91 (2003) 146401.
[23] F. Weigend, R. Ahlrichs, Phys. Chem. Chem. Phys. 7 (2005) 3297.
[24] F. Weigend, Phys. Chem. Chem. Phys. 8 (2006) 1057.
[25] D. Andrae, U. Haeussermann, M. Dolg, H. Stoll, H. Preub, Theor. Chim. Acta 77 (1990) 123.
[26] K. Eichkorn, O. Treutler, H. Öhm, M. Häser, R. Ahlrichs, Chem. Phys. Lett. 240 (1995) 283.
[27] R. Izsák, F. Neese, J. Chem. Phys. 135 (2011) 144105.
[28] S. Grimme, J. Antony, S. Ehrlich, H. Krieg, J. Chem. Phys. 132 (2010) 154104.
[29] S. Grimme, S. Ehrlich, L. Goerigk, J. Comput. Chem. 32 (2011) 1456.
[30] A.V. Marenich, C.J. Cramer, D.G. Truhlar, J. Phys. Chem. B 113 (2009) 6378.
[31] E.S. Boes, P.R. Livotto, H. Stassen, Chem. Phys. 331 (2006) 142–158.
[32] W.R. Fawcett, J. Phys. Chem. B 103 (1999) 11181–11185.
[33] D.H. Wertz, J. Am. Chem. Soc. 106 (1980) 5316–5322.
[34] J. Cooper, T. Ziegler, Inorg. Chem. 41 (2002) 6614–6622.
[35] J. Bernstein, R.E. Davis, L. Shimoni, N. Chang, Angew Chem. Int. Ed. Engl. 34 (1995) 1555–1573.
[36] P. Pertici, G. Vitulli, R. Lazzaroni, P. Salvadori, J. Chem. Soc. Dalton Trans. (1982) 1019–1022.
[37] A. Pastuszko, K. Majchrzak, M. Czyz, B. Kupcewicz, E. Budzisz, J. Inorg. Biochem. 159 (2016) 133–141.
[38] F. Wang, H. Chen, S. Parsons, I. Oswald, J. Davidson, P.J. Sadler, Chem. Eur J. 9 (2003) 5810–5820.
[39] L. Bíró, A. Godó, Z. Bihari, E. Garribba, P. Buglyó, Eur. J. Inorg. Chem. (2013) 3090–3100.
[40] F. Wang, A. Habtemariam, E. van der Geer, R. Fernández, M. Melchart, R. Deeth, R. Aird, S. Guichard, F. Fabbiani, P. Lozano-Casal, I. Oswald, D. Jodrell, S. Parsons, P.J. Sadler, Proc. Natl. Acad. Sci. U.S.A. 102 (2005) 18269–18274.
[41] K.P. Kepp, Coord. Chem. Rev. 257 (2013) 196–209.
[42] G. Skara, B. Pinter, P. Geerlings, F. De Proft, Chem. Sci. 6 (2015) 4109–4117.
[43] G. Skara, M. Gimferrer, F. De Proft, P. Salvador, B. Pinter, Inorg. Chem. 55 (2016) 2185–2199.